NASA TECHNICAL NOTE

NASA TN D-3423

EXPERIMENTAL INVESTIGATION OF MEGAWATT DIRECT-CURRENT ARC HEATING OF NITROGEN

by J. Perry Campbell and Donald R. Boldman

Lewis Research Center
Cleveland, Ohio

NATIONAL AERONAUTICS AND SPACE ADMINISTRATION • WASHINGTON, D. C. • MAY 1966

NASA TN D-3423

EXPERIMENTAL INVESTIGATION OF MEGAWATT DIRECT-CURRENT ARC HEATING OF NITROGEN

By J. Perry Campbell and Donald R. Boldman

Lewis Research Center
Cleveland, Ohio

NATIONAL AERONAUTICS AND SPACE ADMINISTRATION

For sale by the Clearinghouse for Federal Scientific and Technical Information
Springfield, Virginia 22151 – Price $2.00

EXPERIMENTAL INVESTIGATION OF MEGAWATT DIRECT-CURRENT ARC HEATING OF NITROGEN

by J. Perry Campbell and Donald R. Boldman

Lewis Research Center

SUMMARY

Four types of arc heaters, each with the capability of providing arc power levels in excess of 1 megawatt in nitrogen, were tested over a range of power levels and nitrogen flow rates to determine their value as heaters for hypersonic tunnels.

A multiple-chamber arc heater incorporating four magnetically spun direct-current arcs was operated at enthalpy levels of 4000 to 6000 Btu per pound at a nominal pressure of 2.0 atmospheres and nozzle throat diameter of 0.75 inch. The efficiency of this arc heater ranged from about 45 percent at a power level of 600 kilowatts to about 30 percent at 1200 kilowatts.

An arc heater incorporating a gas vortex arc stabilizing mechanism was operated with various nozzles to measure its performance at various pressures for nitrogen flow rates in the range of 0.03 to 0.06 pound per second. This vortex-stabilized arc provided a means of attaining a very high gas enthalpy at modest pressure levels. The maximum enthalpy obtained was 16 500 Btu per pound at a pressure of 1 atmosphere. The flow corresponding to these conditions consisted of a mixture of nitrogen and oxygen at the correct ratio to simulate air; the mixture was injected at a total rate of 0.032 pound per second. Higher pressure runs resulted in lower enthalpies.

A heater incorporating split-ring electrodes which employed both the self-induced magnetic field of the rings and an external magnetic field to rotate the arc was investigated. These split-ring electrodes proved capable of operating at 7000 amperes without burnout and flows of 0.44 pound per second without arc blowout. Arc powers were limited by the physical limitations on the arc gap length, but arc powers of 2.1 megawatts were obtained with a gas power of 866 kilowatts. This maximum power point resulted in an enthalpy of 1900 Btu per pound at a pressure of 11 atmospheres.

A ring-cylinder electrode configuration, which had a 1-inch arc gap, permitted higher powers than the split-ring configuration. The ring-cylinder electrodes carried 7400 amperes without burnout and with these high currents did not blow out until flows of about 0.4 pound per second were reached. Maximum powers obtained were 3.0 megawatts in the arc and 1.2 megawatts in the gas. The corresponding enthalpy was 3400 Btu per pound at a pressure of 11 atmospheres.

INTRODUCTION

A need for the simulation of various aerothermodynamic phenomena occurring in high speed flight and reentry has stimulated research in the field of high powered arc discharges for a number of years. In general, interest has been focused on large scale arc tunnels and therefore on heaters capable of supplying gas powers at megawatt levels. To this end, several heater concepts for the production of high energy gas streams have been investigated by numerous research organizations (ref. 1) with the intent of seeking performance limits and gaining a better understanding of arc discharges. In spite of this large effort, further improvement in the pressure, power level, and enthalpy range for arc heaters is needed to simulate desired flight conditions.

For a particular hypersonic arc tunnel under study at the Lewis Research Center, heaters were desired which were capable of providing enthalpies ranging from 2000 Btu per pound at a flow rate of 1.0 pound per second to 12 500 Btu per pound at a flow of 0.1 pound per second. These conditions correspond to gas powers ranging from 2.11 to 1.32 megawatts, respectively. An additional requirement was that an available low voltage power supply consisting of six direct current generators be used. Four potential arc heater concepts were investigated. These are the multiple-chamber arc heater reported in reference 2, a vortex-stabilized arc heater, a split-ring electrode heater incorporating an additive external magnetic field for rotating the arc, and a heater with ring-cylinder electrodes in which almost all of the arc driving force was furnished by an external magnetic field.

Many parameters affect the performance of an arc heater, and therefore a truly complete picture of an arc heater's performance is difficult to achieve. Also, because of this complexity of the energy transfer within an arc column, theoretical models of electric arcs are scarce, only approximate, and are generally limited to stationary arcs such as that in the vortex-stabilized arc heater. Therefore, the Lewis effort was directed toward experimentally defining the performance limits of these four arc heater concepts which appeared to have the potential of producing the desired high net powers, high stagnation pressures, and high stagnation enthalpies. A secondary goal was a thorough evaluation of each configuration in order to determine optimum operating conditions and provide experience for the design of higher power units.

This work is a comprehensive performance study of these four arc heater designs, one of which has been reported previously. This detailed description of practical experience with such particular schemes should be useful for designing and constructing similar apparatus.

SYMBOLS

A	area
A*	geometric throat area
B	flux density, G
C, C_1	constants
d	diameter, in.
d*	geometric throat diameter
H	enthalpy, Btu/lb
I	current, A
K	constant
L	length
M	mass
$\dot{m}$	flow rate, lb/sec
P	power
p	pressure, atm (unless noted otherwise)
Q	electrical charge
q	heat transfer rate, Btu/(sq ft)(sec)
R	hemispherical nose radius, ft
T	time
V	voltage, V
x	arc length, in.
σ	electrical conductivity
φ, φ_1	nondimensionalized functions

Subscripts:

a	arc
e	nozzle exit
T	total
0	stagnation conditions

2 denotes conditions behind normal shock wave

Superscript:

x denotes nozzle throat conditions

SUPPORT EQUIPMENT

Facilities

The power supply used in the evaluation of the arc heaters covered in this report consisted of six direct-current generators each rated at 600 volts and 1000 amperes but capable of supplying 720 kilowatts for periods of 5 minutes. These generators could be connected in parallel or used independently. Each generator contained a series ballast resistor capable of providing stepwise variations of resistance between 0.15 and 0.33 ohm in 0.03-ohm increments.

Evaluation of the various heater concepts at lower powers was accomplished by using another power supply consisting of two 275-volts, 6000-ampere direct-current generators connected to a series ballast of 0.075-ohm. The ballast of this supply was varied by shorting one or more of the resistance legs, each leg being one-eighth of the total resistance.

All cooling for the high power tests was accomplished with deionized cooling water delivered by a centrifugal pump from a 2500-gallon tank at the rate of 600 gallons per minute. The pump discharge pressure was 1000 psig. The water returned to the tank and was recirculated, thus forming a closed-loop system. A small heat exchanger was used to cool the water; however, the capacity of the heat exchanger was insufficient to maintain a constant water inlet temperature during some of the longer runs with the multiple-chamber arc heater. Inhibited, but not deionized, water at a pressure of 250 psig was used for the lower power tests.

Two 600-ampere welder generators connected in parallel were used for all tests when power for a separately excited external field was required.

Nitrogen gas was supplied at regulated pressures of 300 to 600 psia from either (1) a tube trailer which provided sufficient quantities of nitrogen for numerous runs (up to 5 min/run) at the flow rate of 0.5 pound per second, or (2) a six-bottle supply which limited the run time to approximately 10 seconds at a flow rate of 0.5 pound per second.

Measurements and Instrumentation

The performance evaluation of the arc heaters investigated was based on the computation of gas power by a simple calorimetric technique in which the losses to the coolant are subtracted from the sum of the electrical input power and the power in the inlet gas before heating. The following basic measurements were made for this evaluation:

(1) Arc voltage and current

(2) Inlet gas temperature and pressure

(3) Gas flow rate

(4) Cooling water temperature increase

(5) Water flow rate

Arc chamber pressures and field coil currents were also measured continuously to determine the effect of these parameters on arc performance.

Water flow rates were measured by using calibrated orifice plates and/or turbine-type flow transducers and counter. A commercial differential pressure sensor converted the orifice pressure signal into a flow rate directly readable in units of gallons per minute.

Gas flow rates were determined from recordings of the differential pressure across a subsonic orifice plate (0 to 5 psi for the range of flows investigated) and the orifice upstream pressure which could be regulated up to 500 psi. These two pressures and the arc chamber pressures were converted to electrical signals and recorded on an oscillograph.

The temperature rise of the cooling water through the various arc heater components was measured throughout the arc runs by recording the output signal of copper-constantan thermopiles on an oscillograph. Absolute temperatures were measured by using a precision self-balancing potentiometer and temperature converter sensing the output of iron-constantan thermocouples.

The data presented here were taken from multichannel oscillograph traces to assure simultaneous readings. Because of this, the accuracy of the experimental data is limited to the accuracy of the oscillograph galvanometers (±5 percent).

TEST PROCEDURE

Generally, test runs were made with varying conditions of flow and/or power to obtain the maximum number of data points per run.

Open-circuit voltages were set and the gas flow established at the desired conditions before the arc was struck for all four arc heater configurations. The arc was initiated by the exploding wire technique for all configurations except the vortex-stabilized arc

heater, which was started with a spark starter across the short electrode gap. Once the arc was established, the gas flow was varied throughout the desired range by manual valves and the arc power was varied by varying the generator terminal voltage. The gas flow and/or arc power were varied in steps to assure time for all the instrumentation to respond. The response of the system to parametric variations was limited to the response of the thermopiles, which was under 2 seconds for the magnitude of the step variations established for these tests. After data for the desired range of parameters had been obtained, the tests were generally terminated to conserve the gas supply and limit component wear. Because of this, no time limits on heater performance were established but run times of up to 8 minutes were made with the multiple-chamber arc heater and runs with the vortex-stabilized arc heater were as long as 5 minutes. Both of the configurations using the ring-type electrodes only required runs as long as 50 seconds to complete the full range of parametric variation.

MULTIPLE-CHAMBER MAGNETICALLY SPUN ARC HEATER

Discussion

One approach of obtaining high gas powers is by the utilization of multiple heaters. The performance of such an arc heater comprised of four arc chambers joined to a common plenum is discussed completely in reference 2 and summarized herein.

Configuration

The basic arc heater used was a duplicate of the magnetically spun arc heater described in reference 3. Four of these units, each having a 1-inch-diameter tungsten-tipped cathode and a $2\frac{1}{2}$-inch inside-diameter cylindrical copper anode with an external magnetic field coil for arc rotation, were manifolded together as shown in figure 1.

Results

Preliminary tests on power supply coupling to multiple arcs indicated that the best performance was obtained by connecting a separate generator to each arc chamber of the multiple-chamber heater. Therefore, each arc unit was powered by an independent 1000-ampere, 600-volt generator for all tests of this configuration.

Numerous tests of from 5 to 8 minutes were made at total mass flow rates of from

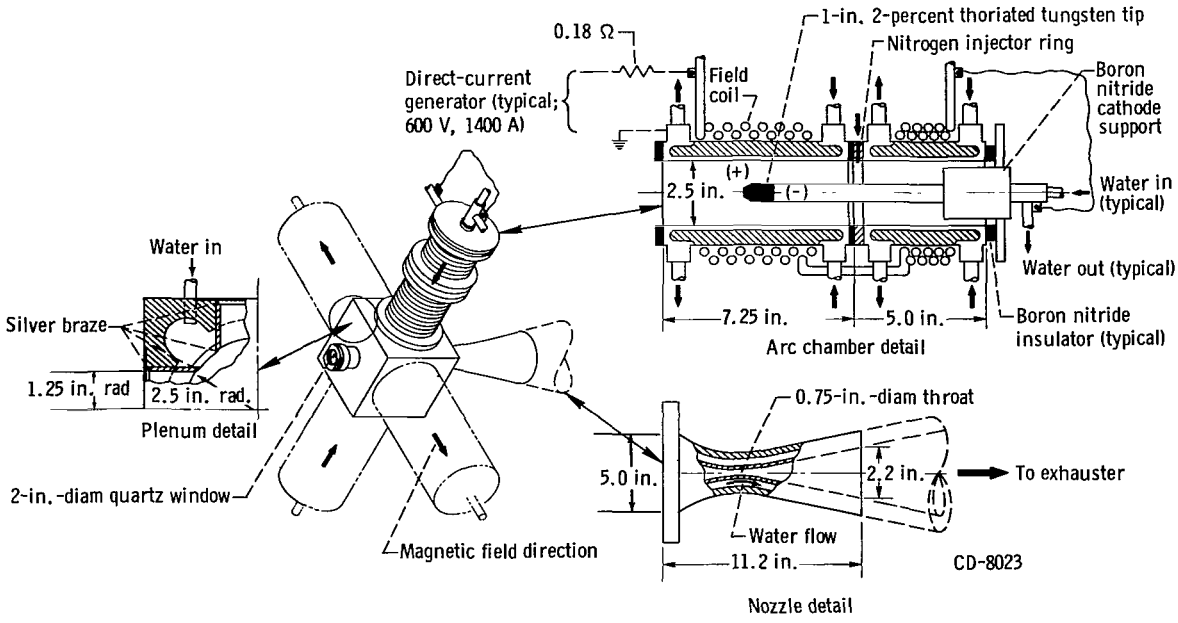

Figure 1. - Multiple-chamber arc heater configuration.

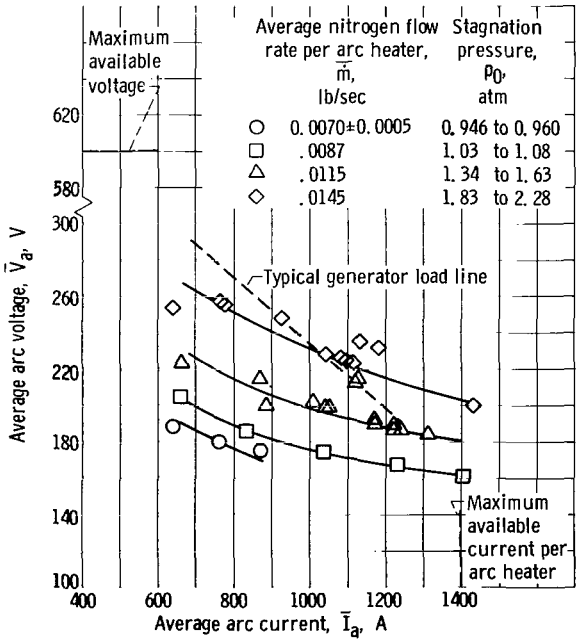

Figure 2. - Voltage characteristics of one arc heater in multiple-chamber configuration as functions of flow rate. Ballast resistance, 0.18 ohm.

0.028 to 0.058 pound per second and at currents of up to 1400 amperes per heater. In all tests the total mass flow rate was equally distributed among the four chambers.

Voltage characteristics. - The average voltage characteristics for the chambers of the arc heater are presented in figure 2 for four different gas flows. These characteristics have a negative slope, that is, the arc voltage decreases with increasing current. The maximum arc potential difference, 260 volts, occurred at the highest mass flow rate; however, extended periods of operation at this condition caused severe erosion of the insulating rings located between the anode and the plenum. The maximum current per arc heater of 1400 amperes was dictated by the power supply. The gas power, as well as the arc power, is continually changing with arc current; therefore, at constant flow rate, the stagnation pressure must also change (approximately as the square root of

gas power). The stagnation pressures indicated in figure 2, for each gas flow rate, correspond to four times the value of nitrogen flow rate indicated since each of the four arc chambers is operating at the same power and flow rate.

Component heat losses and heater efficiency. - The component heat losses are presented in figure 3 for an intermediate and high flow rate of 0.035 and 0.058 pound per second, respectively. As in single heater operation, the electrodes accounted for the major portion of the total loss which was approximately 46 percent of the arc power at the 1-megawatt level. Nozzle losses of 3 percent and plenum losses of 18 percent of the arc power at the 1-megawatt level were observed resulting in a heater efficiency of 33 percent. Shown also in figure 3 is the overall heater efficiency for the high flow case. This efficiency is based on the losses to the electrodes, plenum, and nozzle and does not include power supply and ballast resistor losses. The best efficiency of approximately 40 percent was obtained at a flow rate of 0.058 pound per second and a power of 650 kilowatts.

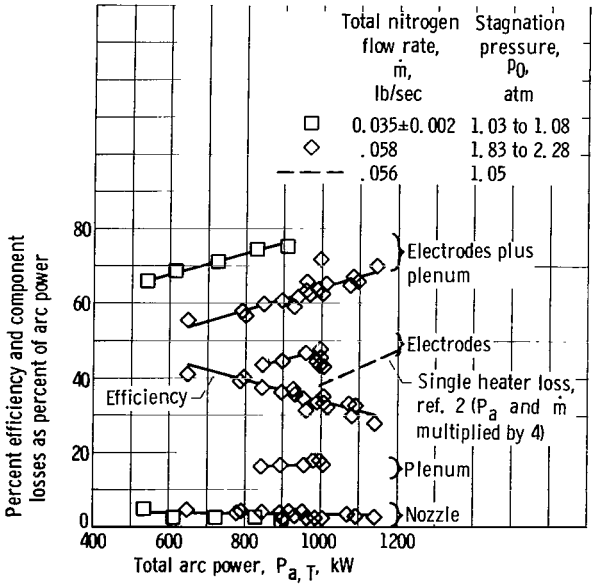

Figure 3. - Component losses and efficiency for multiple-chamber arc.

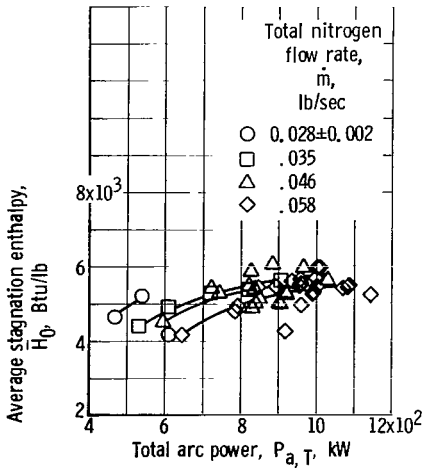

Figure 4. - Variation of stagnation enthalpy with arc power and flow rate for multiple-chamber arc heater.

The electrode losses of a single-arc chamber (ref. 2) are compared to those of the arc chambers in the multiple-heater system operating in a similar environment. In order to make a comparison in one figure between single and multiple-chamber arc performance, the single heater power and flow rate data from reference 2 were multiplied by a factor of 4. If the stagnation pressure and flow rate were identical for the two cases, the curves representing the fractional power losses would be expected to coincide; however, the 0.75-inch-diameter throat of the multiple-chamber arc heater produced pressures slightly higher than those reported in reference 2 for a single heater operating with a 0.50-inch-diameter throat (nominal stagnation pressures of 2.0 and 1.0 atm, respectively). The slightly higher electrode power losses for the multiple

system are attributed primarily to the higher stagnation pressure since the enthalpy levels were nearly equal for the two cases.

Stagnation enthalpy. - Enthalpy levels attained are shown in figure 4, and varied from 4000 to 6000 Btu per pound for the range of flows examined. As was noted in reference 2, the sonic flow correlation of enthalpy given in reference 4 failed to confirm the values determined from energy balance measurements, thus indicating the possibility of departures from the assumed one-dimensional isentropic flow in thermal equilibrium and/or measurement error.

Observations

Steady operation of the arc heater for run times up to 8 minutes (limited only by the coolant system) were obtained by using a separate generator for each arc heater. The nominal stagnation enthalpy was 5500 Btu per pound at a pressure of 2 atmospheres.

The clustering of the heaters provided a means of increasing total gas power in direct proportion to the number of heaters. Based on a comparison of single against multiple heater losses for similar operating environments, it is expected that the gas power of a multiple-chamber system can be predicted from single heater performance at simulated operating conditions provided the plenum heat-transfer rate can be calculated.

The inherent geometrical complexity of multiple chamber systems suggests that the total required power should be achieved with as few arc heaters as possible.

VORTEX-STABILIZED ARC HEATER

Discussion

An investigation of a vortex-stabilized arc heater was undertaken because preliminary studies at Lewis and elsewhere with this type of heater revealed certain potential advantages over the magnetically spun arc heater already discussed. These advantages included (1) higher total power per arc heater, (2) higher stagnation enthalpy for a given flow rate and total power, (3) better compatibility with the available power supply (i.e., arc voltage drop closer to the available 600 V).

Configuration

A schematic of the vortex-stabilized arc heater is shown in figure 5. The electrodes

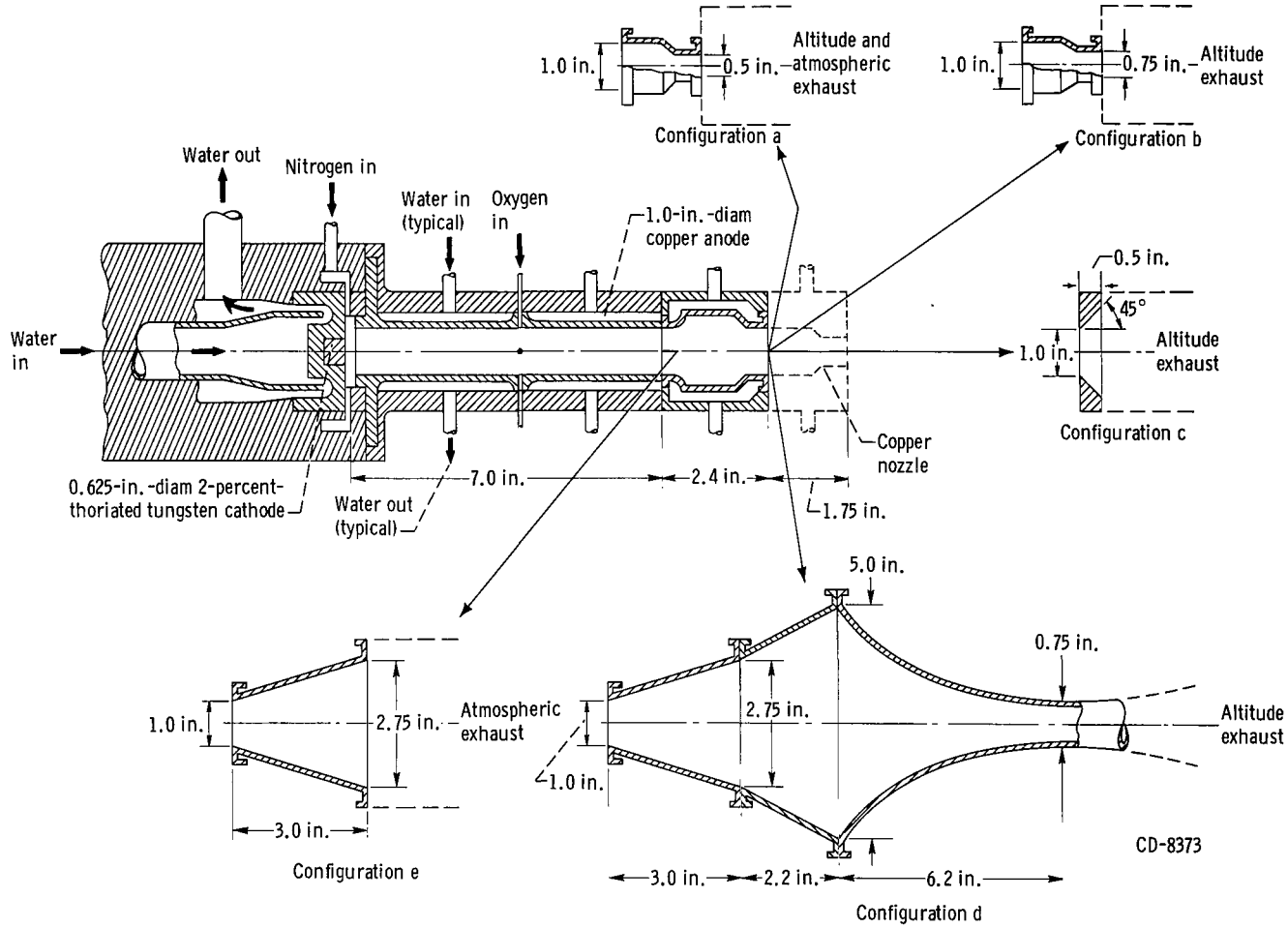

Figure 5. - Schematic of vortex-stabilized arc heater illustrating various nozzle configurations.

consist of 5/8-inch diameter, 2-percent-thoriated tungsten cathode and a 1-inch inside-diameter by a 7-inch-long copper anode. Nitrogen is injected tangentially between the electrodes in order to produce the strong vortex required for stabilizing the arc.

RESULTS

Several nozzle configurations (denoted by a, b, c, d, and e in fig. 5) were tested in order to measure performance over a desired range of pressure and flow. Nozzles a to c were used to study arc behavior in a choked flow environment at pressures in the range of 0.75 to 6.6 atmospheres. Configuration d represents the arc-heater adapter sections in conjunction with the hypersonic arc tunnel nozzle. Nozzle configuration e was used in preliminary tests at atmospheric exhaust conditions in order to gain operational familiarity with the heater. In this latter configuration, oxygen was added to the heated nitrogen in the anode in order to approximate a standard atmospheric mixture of the gases at the exit of the heater. (The direct heating of air yielded prohibitive rates of cathode erosion; therefore, separation of the oxygen and nitrogen was required.)

The upper limit of flow rate for a given nozzle configuration was prescribed by either a power supply voltage limitation (characteristic of configurations a, b, and d in fig. 5) or the inability to control the length of the arc (noted with configurations c and e in fig. 5). The lower limit of flow rate for maintenance of a stable arc was established from past experience. As the mass flow rate is reduced, a lower limit is reached beyond which a sudden contraction in the length of the arc results in electrode burnout. This lower limit was nominally 0.02 pound per second at atmospheric pressure for an arc power of 1 megawatt. The safe lower limit rate increased slightly with pressure; however, for the range of conditions investigated in this study, it was always less than 0.03 pound per second.

Voltage characteristics. - The voltage characteristics for the vortex-stabilized arc exhibit a zero to positive slope (as shown in figs. 6(a) to (d)). The positive slope is particularly desirable because the ballast resistance required for a stable discharge can be reduced or eliminated. For the 1/2- and 3/4-inch-diameter nozzles, the positive characteristic is obtained and is quite pronounced (figs. 6(a) and (b)).

The increase in voltage with current for a constant flow rate and given geometry is accompanied by an increase in arc chamber pressure. The range of pressure obtained for a given flow rate is indicated in figure 6, with the lowest and highest pressures corresponding to the lowest and highest arc current, respectively.

Observation of the voltage characteristic curves for flow rates of 0.025 and 0.035 pound per second in figure 6(a) reveals that at constant current the voltage was higher for runs incorporating an atmospheric rather than the low pressure altitude exhaust system.

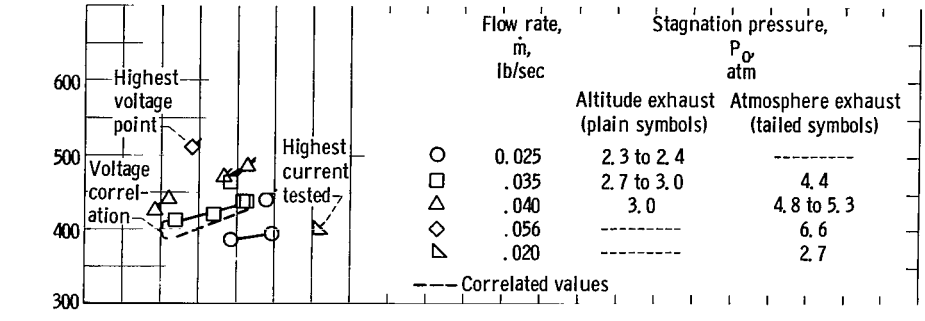

(a) Configuration a. Throat diameter, 0.5 inch; altitude and atmospheric exhaust.

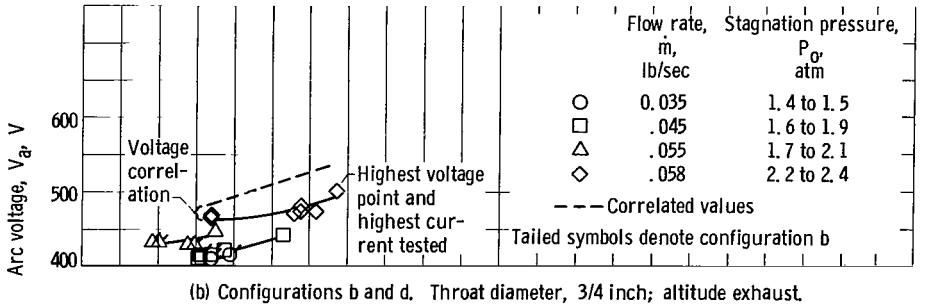

(b) Configurations b and d. Throat diameter, 3/4 inch; altitude exhaust.

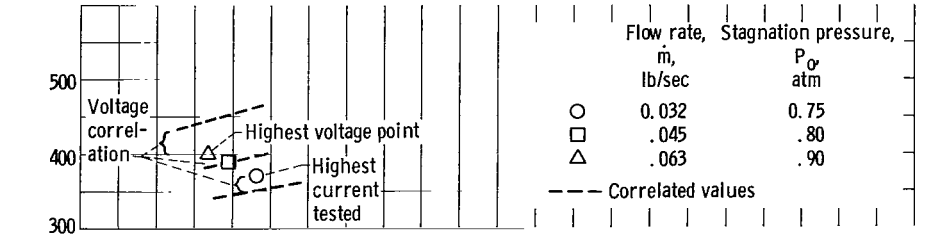

(c) Configuration c. Throat diameter, 1.0 inch; altitude exhaust.

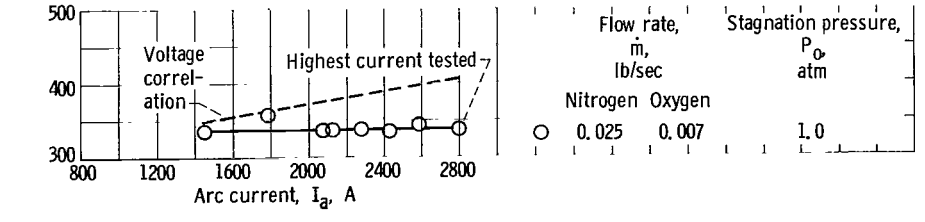

(d) Configuration e. Throat diameter, 1.0 inch; atmospheric exhaust.

Figure 6. - Voltage characteristics for various configurations of the vortex-stabilized arc.

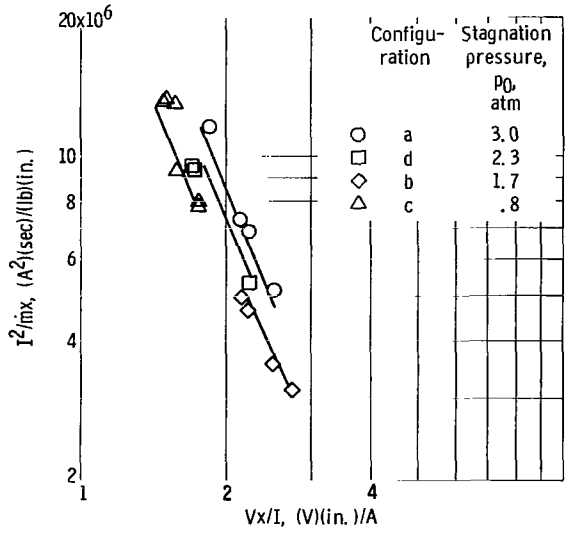

Figure 7. - Dimensionalized characteristic variables at constant stagnation pressure for vortex-stabilized arc.

A voltage correlation can be obtained for the vortex-stabilized arc by modifying the dimensional correlation presented in reference 5 to include the influence of stagnation pressure (see appendix A). This stagnation pressure effect on the dimensional variables is shown in figure 7. The correlation yields the following empirical equation (denoted as (A3) in appendix A):

$$\frac{I^2}{\dot{m}x} = 3.56\times10^7\left(\frac{Vx}{I}\right)^{-2.61} p_0^{0.338} \qquad (1)$$

Arc voltage characteristics predicted by equation (1) are shown in figures 6(a) to (d). The correlated values of voltage are based on the experimental values of arc current, flow rate, and stagnation pressure. In figures 6(a), (b), and (c), the correlation agrees with the experimental voltage to within approximately 10 percent. In figure 6(c), the trend of the voltage was obtained by differentiation of voltage in equation (1) with respect to current at the current corresponding to each data point. In figure 6(d), the deviation from measurements at high arc currents could be attributed to several factors. For instance, the flow was comprised of a mixture of nitrogen and oxygen rather than nitrogen for which the correlation was derived. Also, with configuration 5(e), the plenum section was not used; therefore, the arc was free to change length.

Although insufficient data are available to establish the limitations of this correlation, the dimensional analysis technique of reference 5 is a relatively simple and useful method of correlating vortex-stabilized arc discharge parameters. It is expected that by incorporating in the vortex arc heaters an electrically neutral tube between the electrodes, thereby confining the arc length to an accurately known constant value, the correlation could be greatly improved.

Component heat losses and heater efficiency. - In figure 8, the component heat losses are shown for configurations a, b, and c operating at flow rates of 0.032 to 0.035 pound per second. Cathode losses were less than 4.0 percent of the arc power and nozzle losses were nominally 5.0 percent of the arc power. The most significant change in heat loss occurred in the anode. For instance, at an arc power of 600 kilowatts, the anode fractional loss ranged from 25 percent at a pressure of approximately 0.8 atmosphere (configuration c) to 45 percent at a pressure of 2.8 atmospheres (configuration a). Corresponding heater efficiencies were 73 and 46 percent, respectively. It will be shown

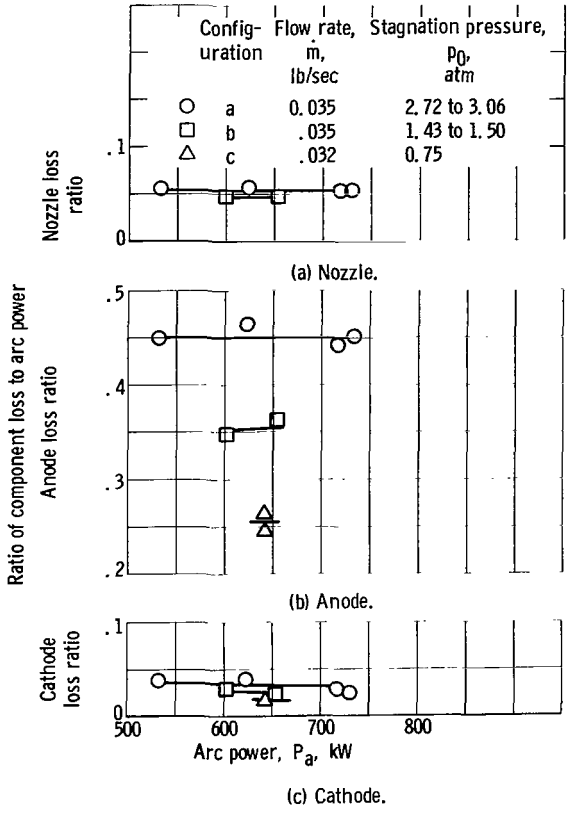

Figure 8. - Component heat losses for vortex-stabilized arc.

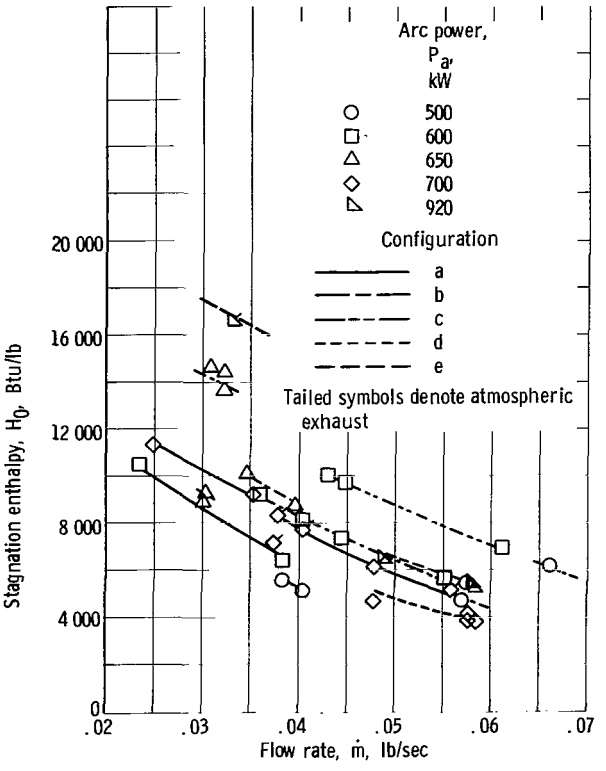

Figure 9. - Stagnation enthalpy variation with flow rate at constant arc power for various configurations of vortex-stabilized arc. (Enthalpy based on losses to electrodes and nozzle.)

in the following section that the marked decrease in the anode heat loss at low pressure results in very high values of stagnation enthalpy ($H_0 > 10\ 000$ Btu/lb).

Stagnation enthalpy. - The variation of stagnation enthalpy with flow rate at constant values of arc power is shown in figure 9 for arc heater configurations a, b, c, d, and e shown in figure 5 (p. 10). A nearly linear reduction in stagnation enthalpy with increasing flow rate can be noted. The maximum value of stagnation enthalpy (16 500 Btu/lb) was obtained with configuration e, operating at an arc power of 940 kilowatts and a pressure of 1.0 atmosphere. The current at this power level was 2800 amperes, which represents approximately the upper limit for the cathode at atmospheric pressure. It is expected that higher values of enthalpy could be obtained at this current by reducing the stagnation pressure level, since, as shown in the previous section, the anode loss can be greatly reduced by lowering the pressure. This conclusion tends to be substantiated by the results presented in references 6 and 7 in which electrode geometries are similar and the stagnation pressures are low ($p_0 < 1.0$ atm). It is also interesting to note that the stagnation enthalpy for the vortex-stabilized arc varies linearly with arc current for constant mass flow rates. This condition is shown in figure 10 for configuration e operating at a flow rate of 0.032 pound per second of nitrogen and oxygen. Such a linear variation

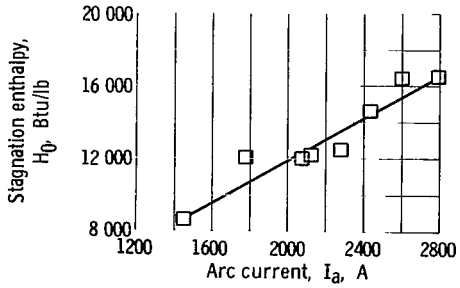

Figure 10. - Stagnation enthalpy variation with arc current for configuration e operating at constant flow rate. Flow rate, 0.032 pound per second ($N_2 + O_2$).

for this case is predicted by the equations of reference 8. This linearity was obtained even though the vortex-stabilized arc in this investigation differs from the model used in the analysis of reference 8.

SPLIT-RING ELECTRODES HEATER

Discussion

In each of the two arc heater configurations already discussed, the current limit of the electrodes, namely the thoriated tungsten cathodes, is below the 6000-ampere nominal supply that was available. Thus, to take full advantage of the available power, multiple units are required. Because of the greater simplicity and in keeping with the recommendations of reference 2, a single arc heater was sought that would be capable of carrying the full current of our power supply.

Preliminary studies with water-cooled copper ring electrodes had indicated their ability to handle currents of 6000 amperes or more; hence, the development of a single arc heater using these "cold" rings as the electrodes was an attractive possibility.

One type of these "cold" cathode arc heaters is the split-ring electrode configuration reported in reference 9. The magnetic driving force for these electrodes is essentially the same as that used in rail accelerators. The power leads must be applied to only one of the stems of each electrode and in such a manner that the current in the rings flows in opposite directions. Thus the magnetic fields set up by the current in the rings are additive in the region between the rings and will react with the current in the arc itself to provide the arc rotational driving force. The splits of each electrode are displaced angularly from each other, because the self-induced field contribution from each ring is zero immediately after the split is jumped.

The self-induced magnetic field in the region between the rings varies according to the position of the arc on the electrodes since the length of the current path in the rings varies with arc position. Approximate expressions for the magnetic field of a partial loop current are derived in appendix B for points in the plane of a partial loop, both inside and outside the arc of the partial loop current. These expressions were needed to evaluate the magnitude of the self-induced field of this configuration. A plot of the magnetic field strength, based on these expressions, for the midpoint of the arc is presented in figure 11 for a 0.46-inch arc gap and a 6000-ampere arc current.

Since the stems of the electrodes are at right angles to the rings, the driving force on the arc is considerably less immediately after jumping the split, as indicated by the

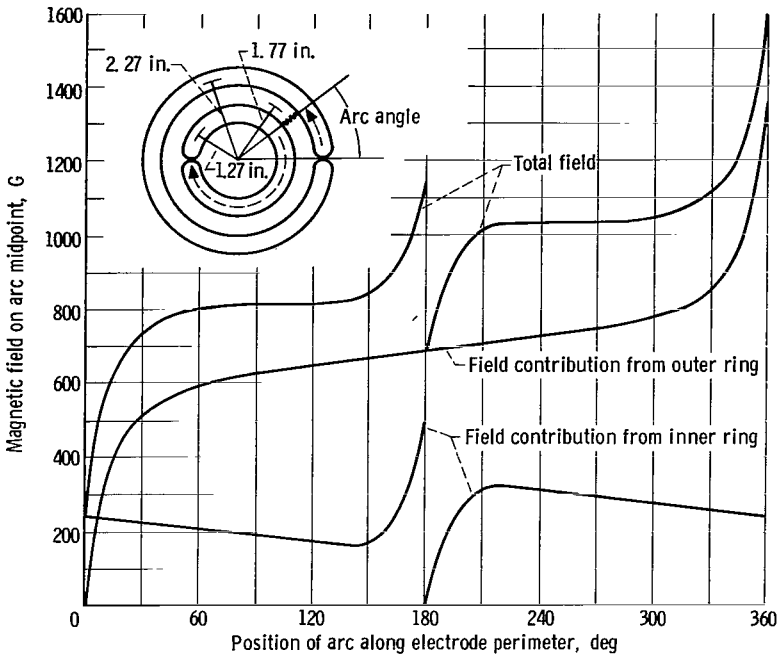

Figure 11. - Self-induced magnetic field on arc midpoint with an arc current of 6000 amperes for one split-ring configuration.

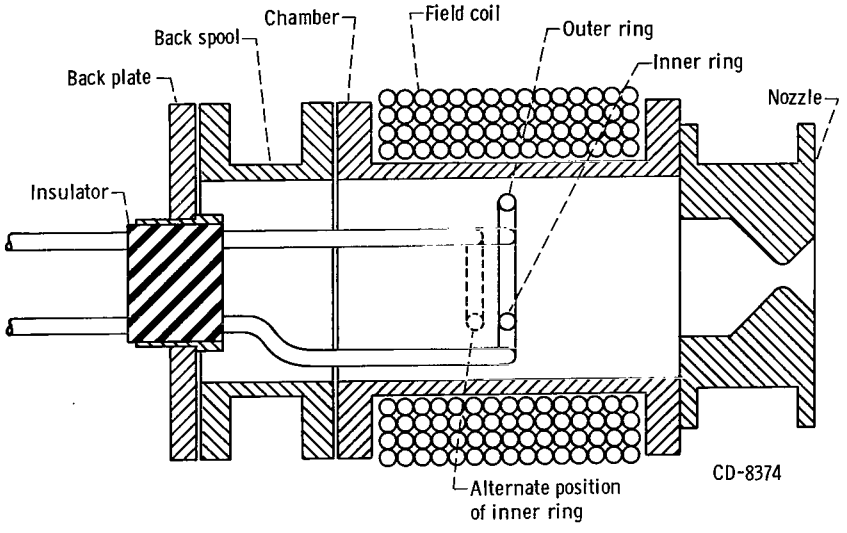

Figure 12. - Split-ring electrode arc heater. (Cooling passages, gas ports, and seals are not indicated.)

dip in field strength at the zero and 180° position of the arc on the electrodes. Because of this, the region of the splits is subject to greater erosion than the rest of the rings. Therefore, in an effort to increase the velocity of the rotating arc in general and especially at the high erosion point of the splits, it was decided to apply an external field that would tend to drive the arc in the same direction as the self-induced magnetic field. The method chosen to accomplish this was to immerse a coplanar split-ring electrode configuration in an external axial magnetic field (see fig. 12).

Configuration

The concentric, coplanar split-ring electrodes used (fig. 13) were designed to be mounted in an available water-cooled copper test chamber which had provisions for applying an axial magnetic field. Part of this test chamber (shown in fig. 12) was originally designed as an anode for another arc heater. It had a cylindrically shaped inner surface 6 inches in diameter and 9.88 inches in length and was wrapped with a field coil formed by four layers of fifteen turns per layer of polyethylene insulated 3/8-inch copper tubing. A cylindrical extension that increased the cavity length 4 inches and an end plate were also fabricated for the split-ring tests. A water-cooled nozzle section with 45° convergent entrance and a throat diameter of 3/4 inch was adapted to the 6-inch chamber to simulate the 3/4-inch throat diameter nozzle of the tunnel on which the heater was intended to be used.

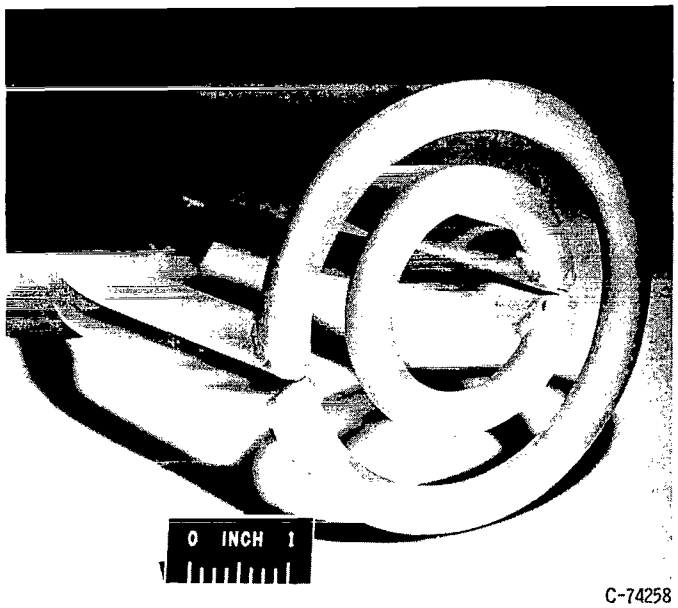

Figure 13. - Split-ring electrodes.

It was not possible to power the field coil by placing it in series with the arc, as was done in previous tests, because the cooling system limited the coil current to about 1500 amperes, whereas the full 6000 amperes was desired for the electrode tests. Consequently, it was decided to excite this coil by two 600-ampere direct-current welder generators connected in parallel with a common control. Almost all of the split-ring tests were made with 1200 amperes in the field coil, which gave a magnetic field value of 3240 gauss on the midpoint of the coil axis.

The end plate used to seal the end

of the chamber had provisions for gas injection into the chamber through eight equally spaced 0.196-inch inside-diameter tube inlets on a 4.88-inch-diameter circle. Each inlet tube was bent so as to impart a tangential swirl to the incoming gas opposite to the direction of arc rotation. During the test program these inlet tubes were replaced with straight pipe inlets to give an axial inlet flow, since reference 10 noted higher efficiencies with such a flow.

The end plate also had a cylindrical sleeve cavity, 3.50 inches in diameter and 2.50 inches long, mounted through its axis as shown in figure 12. This cavity was used to hold an insulator made of unfired lava (aluminum silicate) designed to support the stems of the split-ring electrodes.

Sets of electrodes were fabricated from 1/2-inch copper tubes (0.062-in. wall) and from two different wall thicknesses (0.082 in. and 0.123 in.) of 1/4-inch commercial copper pipes (0.540-in. o.d.). The rings were formed with inside diameters of 2 and 4 inches and fastened to the electrode stems, which were perpendicular to the plane of the rings, by copper welding mitered joints. The splits were maintained as close as practical (approximately 1/32 in.) without actually touching. Figure 13 shows a set of these rings mounted in the lava insulator.

Results

The first aim of this split-ring test program was to establish the current limits of the various electrodes and then increase these limits to and beyond the current limits of the power supply. The rings were mounted concentric with the axis of the chamber and at the midpoint of the field coil. With 375-psig cooling water pressure on the electrodes and 1000 amperes in the field coil the arc current was steadily increased until burnout occurred.

The 0.062-inch wall tube and the 0.082-inch wall pipe electrodes failed by burnout at about 4800 amperes while the 0.123-inch wall pipe burned out at 6500 amperes. Water flow rates through the electrodes were approximately 2.7 pounds per second for the tube and thinner wall pipe and 2.0 pounds per second for the heavy wall pipe, which corresponds to linear speeds of 56.2 and 68.1 feet per second, respectively, for coolant flow through the electrodes.

All burnout points occurred on the larger ring (which has the higher arc root velocity) and just beyond the stem on the water inlet side of the ring, where the water temperature should be the lowest. One possible explanation for this would be separation of the water flow from the tube wall during the sharp bend from the stems into the rings. Cavities which result from this flow separation would tend to occur on the inside wall of the bends, where the arc also occurs. Separation in the smaller ring, while probably more severe

than in the larger ring, would occur on the side of the ring away from the arc root.

One method of increasing the current limit of the split-ring electrodes was to increase the water pressure on the rings to 800 psig. Besides increasing the coolant flow rate through the rings and improving the cooling in general, the increased pressure would decrease the tendency of the flow to separate and increase the boiling point of the coolant.

The higher pressure, which gave water flow rates through the electrodes of 3.6 pounds per second for the 0.062-inch wall tubes and 0.082-inch wall pipe and 3.1 pounds per second for the heavy wall pipe, permitted running the tube electrodes at currents as high as 5800 amperes without a burnout while the heavy wall pipe electrodes were operated at currents up to 6800 amperes without visible erosion.

Cooling water flowed through the electrodes opposite to the arc rotation direction in order to reduce the possibility of local boiling at the arc root.

Another method of dealing with the cavitation problem consisted of replacing the copper-welded mitered joints with commercial cast brass tubing elbows which have formed smooth flow passageways. This resulted in the loss of some of the roundness of the rings, especially on the smaller rings. These elbows worked quite well in preventing burnout. However, they were quite prone to develop pin hole leaks, probably because of the porosity of the cast brass.

A systematic investigation of the effect of field strength on arc power was not attempted, but the few tests conducted with different and varying field excitation indicated a decrease in arc power with decreasing field strength for given values of arc current and mass flow rate.

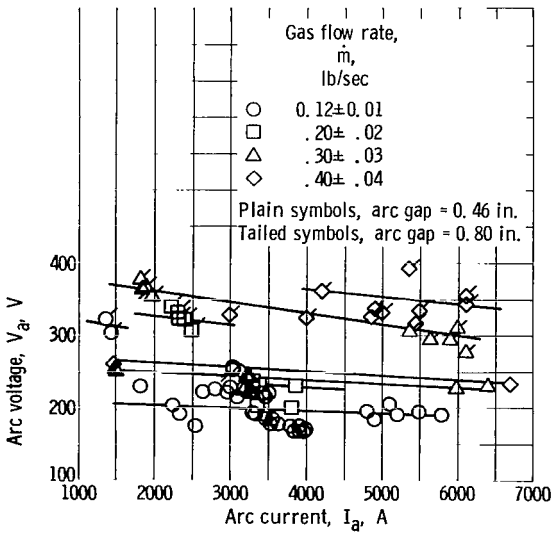

Figure 14. - Arc characteristic for split-ring configuration.

The split-ring electrode provides a convenient method of counting arc rotations. The voltage drop through the ring itself is recorded by applying an oscilloscope across the split and photographing a single sweep of the scope during arc operation. Systematic study of arc rotation frequencies was not attempted, but rotational frequencies for the various flows, powers, and gaps studied ranged from 2000 to 3000 cycles per second.

Voltage characteristics. - The voltage characteristics for the range of currents and gas flows investigated with coplanar split-ring electrodes are presented in figure 14 by the plain symbols. There was some scatter in the voltage characteristic between different

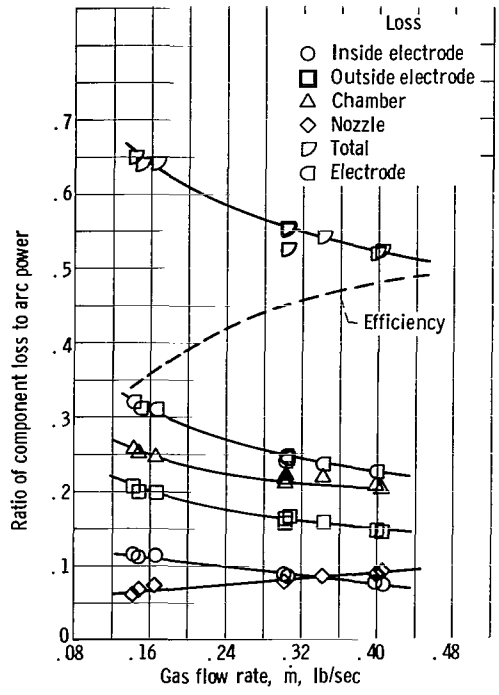

Figure 15. - Component heat losses and efficiency for split rings. Arc gap, 0.80 inch; arc power, 1600±100 kilowatts.

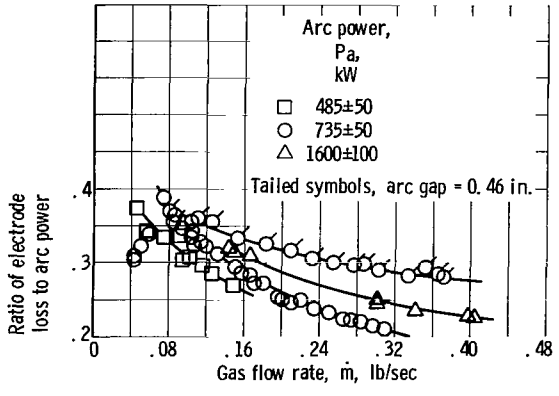

Figure 16. - Electrode heat losses for split rings with 0.80- and 0.46-inch arc gaps.

runs which might have been caused by eccentricities in the electrode spacings or changing condition of the electrode surfaces. Generally however, the characteristics for each similar flow rate exhibits a flat to slightly negative slope over this current range. Varying the flow rate from 0.11 to 0.44 pound per second changed the arc voltage from 175 to 260 volts.

The geometry of the cylindrical chamber limited the size of the larger ring electrode and hence the arc gap distance for coplanar rings. In an effort to increase the arc voltage for a given flow condition, the arc gap was increased by displacing the rings axially as indicated by the dotted electrode in figure 12 (p. 16). The inner ring was stationed 0.90 inch upstream from the outer ring keeping the arc on the midpoint of the field coil.

The increased arc voltage, using this longer gap, noncoplanar spacing is indicated in figure 14 by the tailed symbols where for the same range of gas flows and arc currents the arc voltage ranged from 300 to 390 volts.

Although this offsetting of the plane of the rings had the desired effect of increasing arc voltages, it should be pointed out that this method of increasing gap length results in lower driving fields. The increased separation reduces the self-induced field and the external field is reduced in effectiveness because it is no longer normal to the arc. This lower field might result in lower current limits for the electrodes. However, the 0.123-inch wall pipe electrodes were operated in this configuration at currents of up to 6000 amperes without a burnout.

Component heat losses and heater efficiency. - The losses and heater efficiency are presented in figure 15 for a range of gas flows of 0.14 to 0.40 pound per second with an arc power of 1600 kilowatts and an arc gap of 0.80 inch. These curves, which are typical for the range of arc powers investigated, indicate the improvement in heater efficiency with increasing gas flow as the overall efficiency went from 35 percent at the low flow to

48 percent at the highest flow. The nozzle loss was the only component loss that increased with increasing flow, going from 6 to 9 percent of the input arc power.

The effect of arc power on component heat loss and heater efficiency is indicated in figure 16. Electrode losses for the three different arc powers show the increase in heater loss percentage of arc power with increasing arc power.

Stagnation enthalpy. - The ranges of variation of the gas flows and arc powers with the resulting enthalpies for the split-ring tests are indicated in figure 17(a) for the 0.46-inch arc gap and in figure 17(b) for the 0.80-inch arc gap. The maximum gas flow during these tests was 0.44 pound per second and the maximum arc power was 2100 kilowatts.

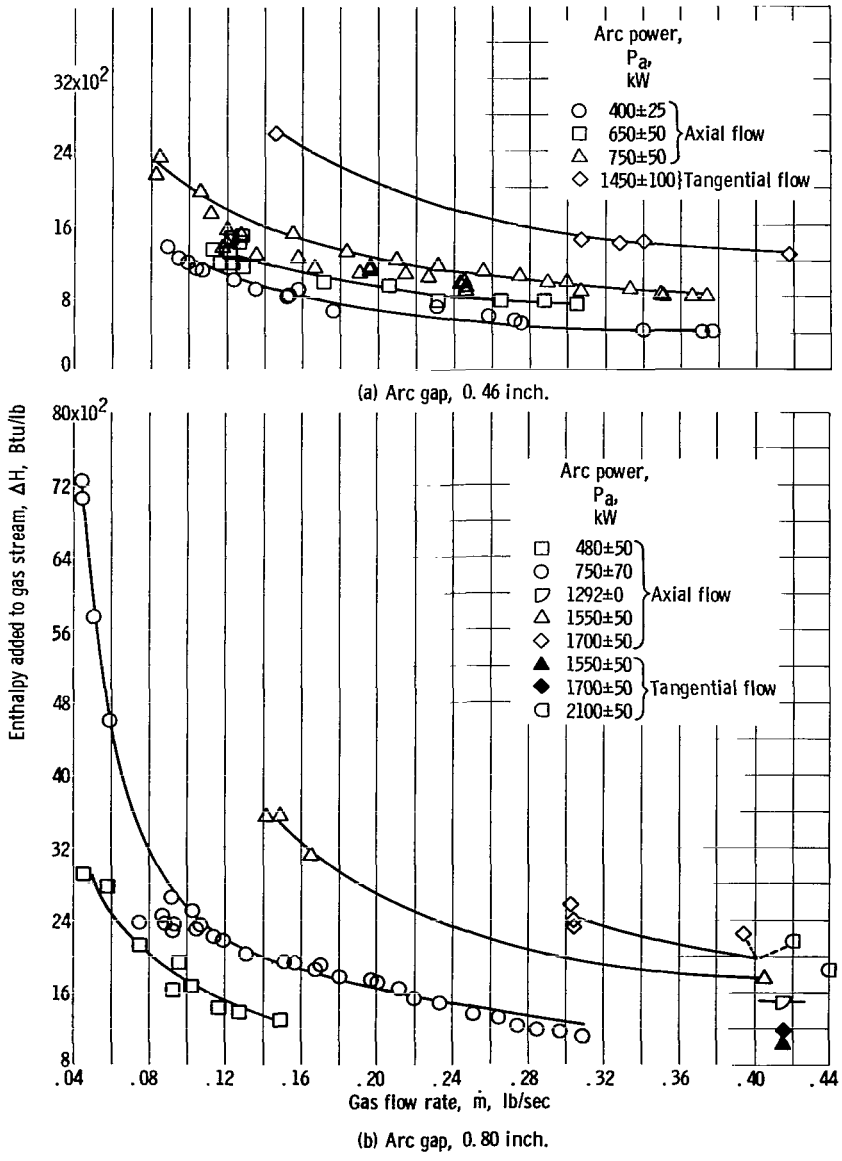

Figure 17. - Enthalpy as function of gas flow at constant arc power for split rings.

Neither of these values is necessarily the configuration's maximum value since the heater still operated at this point without electrode burnout or arc blowout. The gas flow was limited by the constrictions in the gas manifold ring and the power was limited by the generator approaching its maximum voltage. Both of these might have been increased by increasing the manifold size and reducing the ballast and hence the ballast drop permitting a larger voltage drop in the arc itself.

The gas injection was axial for most of the data reported in figures 17(a) and (b) with a few points from the earlier tangential injection scheme shown to indicate the improvement in performance at a given input power with the axial injection, as was also noted in reference 10.

Figure 18 indicates the more efficient heating of the longer arc for the same arc power because of the higher voltage inherent in the longer arc. For the two similar arc powers shown, the 0.80-inch arc gap gives from 400 to 600 Btu per pound more enthalpy than the 0.46-inch arc gap at the same gas flow rate. Thus, the longer arc gap not only permits higher arc powers without exceeding the current limit of the electrodes but it improves the performance of the heater as well.

Arc chamber pressures for the range of flows and arc powers investigated are shown in figure 19(a) for the 0.46-inch arc gap case and in figure 19(b) for the 0.80-inch arc gap case. The cold flow pressures are also presented and compared with a one-dimensional, isentropic, sonic flow equation.

As would be expected, the pressure level in the arc chamber increases with increasing gas flow and with increasing arc power.

Observations

The limited tests performed with the split-ring electrode heater indicate that this approach to arc heating of gas at high power levels is quite promising.

Split-ring electrodes fabricated of commercial copper pipe proved capable of operating at 6800 amperes without burnout and flows of 0.44 pound per second without blowout. Arc powers of 2.1 megawatts were obtained with resulting gas powers of 866 kilowatts and heating efficiencies of 41 percent.

The external magnetic field proved effective in preventing erosion at the splits of the rings, the wear point in ordinary split-ring electrodes. However, the physically large coil for this external field reduces one of the advantages of ordinary split-ring electrodes over ordinary magnetically spun arcs, which is elimination of the bulky field coil. This bulk could perhaps be greatly reduced by providing a small shaped external field only in the region of the splits, where it is most needed.

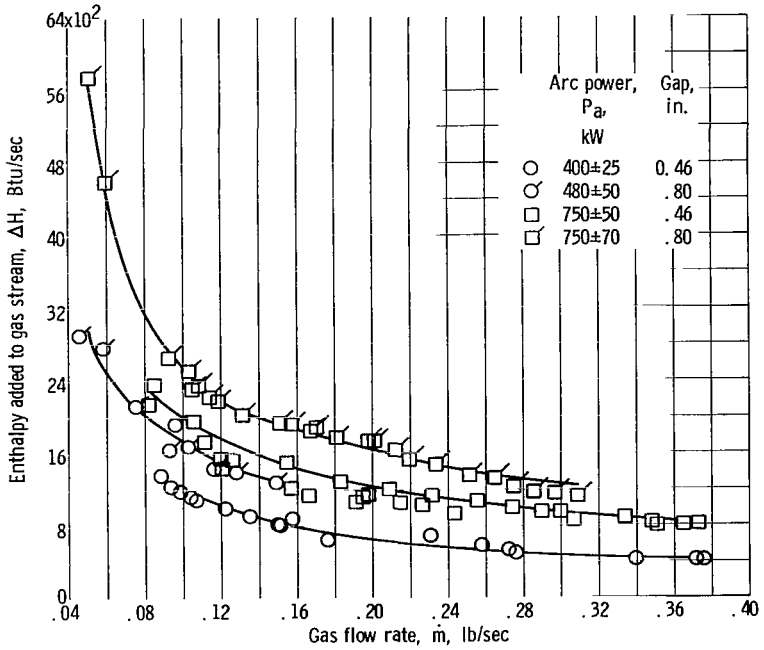

Figure 18. - Enthalpy as function of gas flow at constant arc power for two arc gaps of the split-ring configuration.

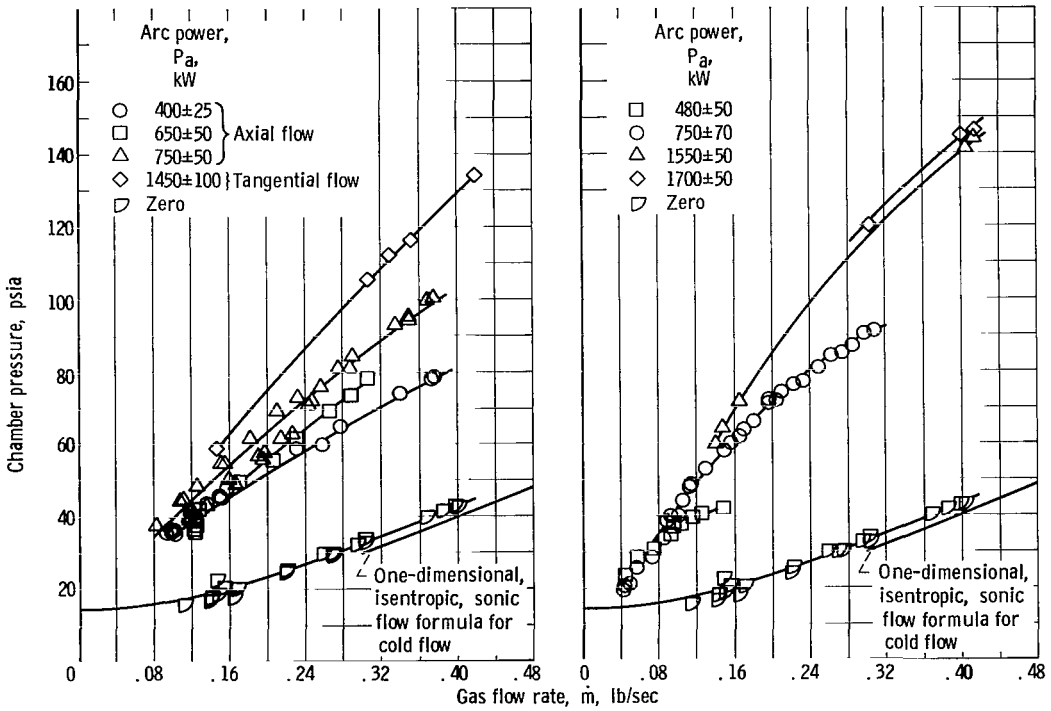

(a) Arc gap, 0.46 inch.

(b) Arc gap, 0.80 inch.

Figure 19. - Chamber pressure as function of flow rate at constant power.

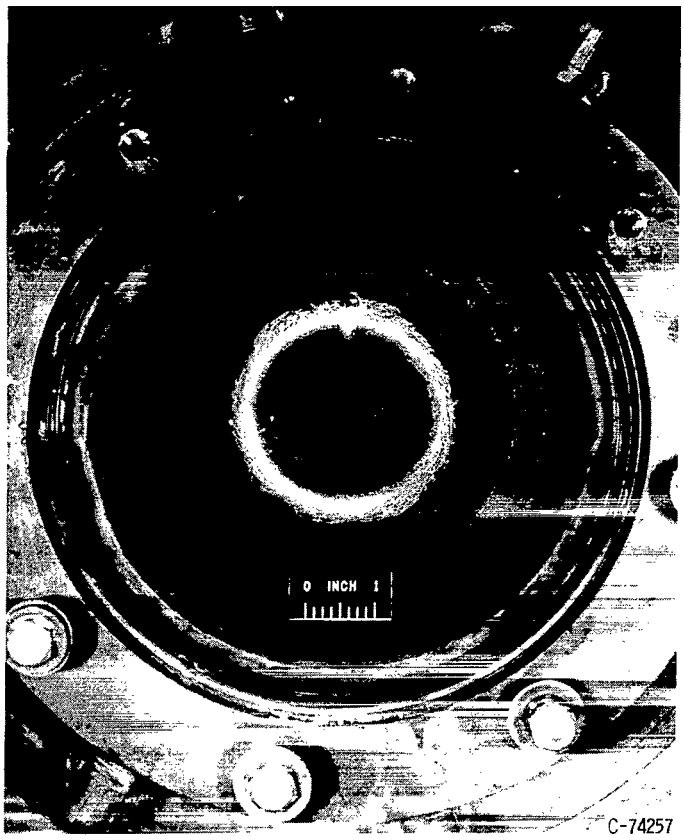

Figure 20. - Ring-cylinder configuration.

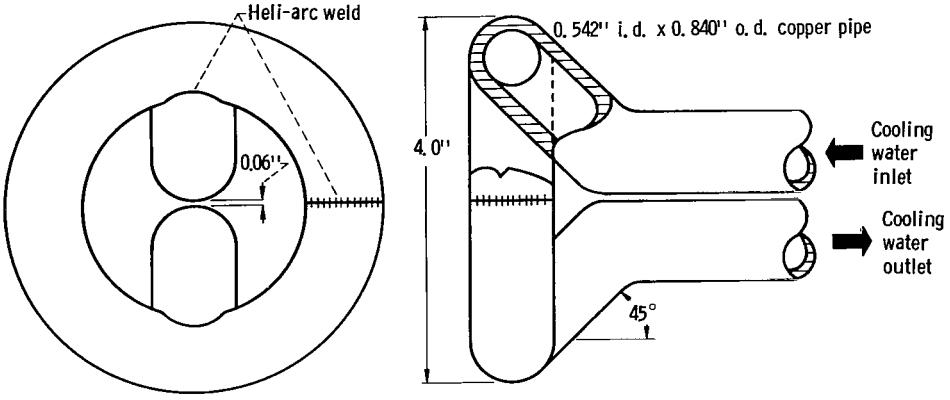

Figure 21. - Schematic of ring electrode.

RING-CYLINDER ELECTRODES HEATER

Discussion

Another electrode configuration that looked promising from preliminary tests with no gas flow was the ring inner electrode and the cylinder outer electrode shown in figure 20. This configuration depends entirely on an external field to drive the arc, as in the first configuration, but both electrodes operate "cold" as in the third configuration.

Configuration

The water-cooled chamber with associated field coil used for the split-ring electrodes test was used to provide the cylindrical outer electrode and the driving force field for the ring-cylinder configuration. The inner ring electrode was fabricated from 1/2-inch commercial copper pipe (0.840-in. o.d., 0.149-in. wall thickness) bent into a copper-welded closed ring with an outside diameter of 4 inches. Cooling water inlet and outlet tubes were copper welded to the ring 180^{o} apart as indicated in figure 21. These tubes were mounted in a brass sleeve and installed in a lava insulator similar to the one used for the split-ring tests. The ring of this electrode was mounted concentric with the chamber, that was being used as the other electrode, and at the midpoint of the field coil which gave an arc length of 1 inch. All other components of this configuration were the same parts as used for the split ring, with axial gas injection.

Results

With 840-psig water pressure, which gave approximately 6 pounds per second of flow through the ring, and with 1200 amperes in the field coil, these electrodes proved capable of running at currents of 7000 amperes without burnout although pin-hole leaks in the ring did occur. The lava insulator for the ring-cylinder configuration eroded much more than for the split-ring configuration, probably due to the higher powers attained with the ring cylinder. A shield of asbestos board fastened to the chamber end of the insulator successfully checked this erosion.

All of these tests with the simulated nozzle section attached were made with 1200 amperes in the field coil which gave a magnetic field value of 3240 gauss on the midpoint of the coil axis. Earlier tests of this configuration for the purpose of studying arc rotation behavior were made with an open chamber, no gas flow and field excitation currents of 1000, 800, 600, 400 and 200 amperes. Arc rotation rates were measured by photo-

graphing from an oscilloscope the output of a photo diode that received its signal from only one side of the annular arc gap.

Voltage characteristics. - The voltage characteristics for three typical gas flow rates over the range of current investigated with the ring-cylinder electrodes are presented in figure 22. As with the split-ring electrodes there was some scatter in the voltage characteristic between different runs which might have been caused by eccentricity of the ring electrode spacing inside the cylinder or the changing condition of the electrode surfaces. Generally, however, the characteristics exhibit slightly negative slopes over this current range. Voltages were generally between 250 and 400 volts with the higher voltages being associated with the higher flows.

The voltage characteristics for this con-

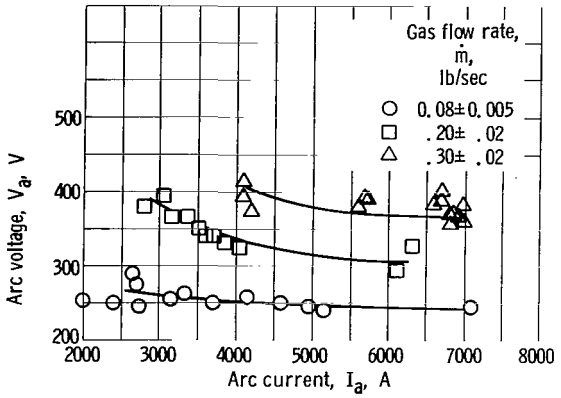

Figure 22. - Arc characteristic for ring-cylinder configuration.

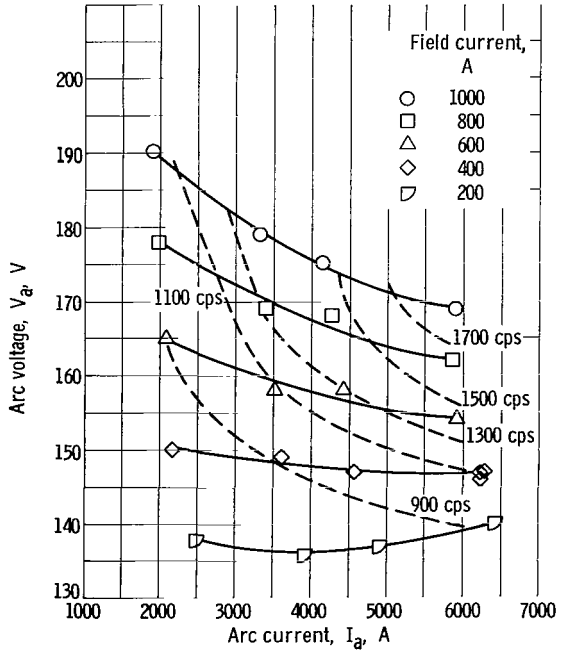

Figure 23. - Arc characteristics and rotation rates for different field excitations of ring-cylinder configuration with no flow and at atmospheric pressure.

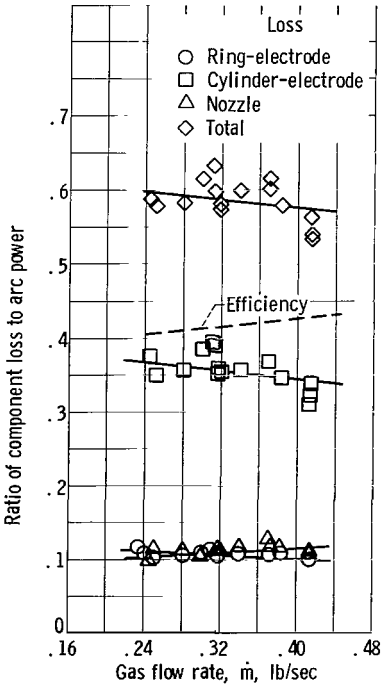

Figure 24. - Component heat losses and efficiency for ring cylinder. Arc power, 2500±100 kilowatts.

figuration with no gas flow and atmospheric pressure are presented in figure 23 for five different magnetic field strengths. These voltages were between 135 and 190 volts with the higher voltages being associated with the higher field. While these runs were with no gas flow a similar trend would be expected for runs with gas flow. The arc rotational frequency for each data point was also recorded and a cross plot of constant arc frequency is shown. Frequencies from 500 to 1850 cycles per second were recorded with the highest frequency being at the highest field strength and the highest arc current.

Component heat losses and heater efficiency. - The losses and heater efficiency are presented in figure 24 for a range of gas flows of 0.24 to 0.42 pound per second with an arc power of 2500 kilowatts. These curves which are typical for the range of arc powers investigated, indicate a slight improvement in heater efficiency with increasing gas flow as the overall efficiency went from 40.5 percent at the low flow to 43.0 percent at the highest flow. Like the split-ring electrode configuration, the nozzle loss was the only component loss that increased with increasing flow.

Stagnation enthalpy. - The ranges of variation of the gas flows and arc powers with the resulting enthalpies for the ring-cylinder tests are shown in figure 25. The maximum

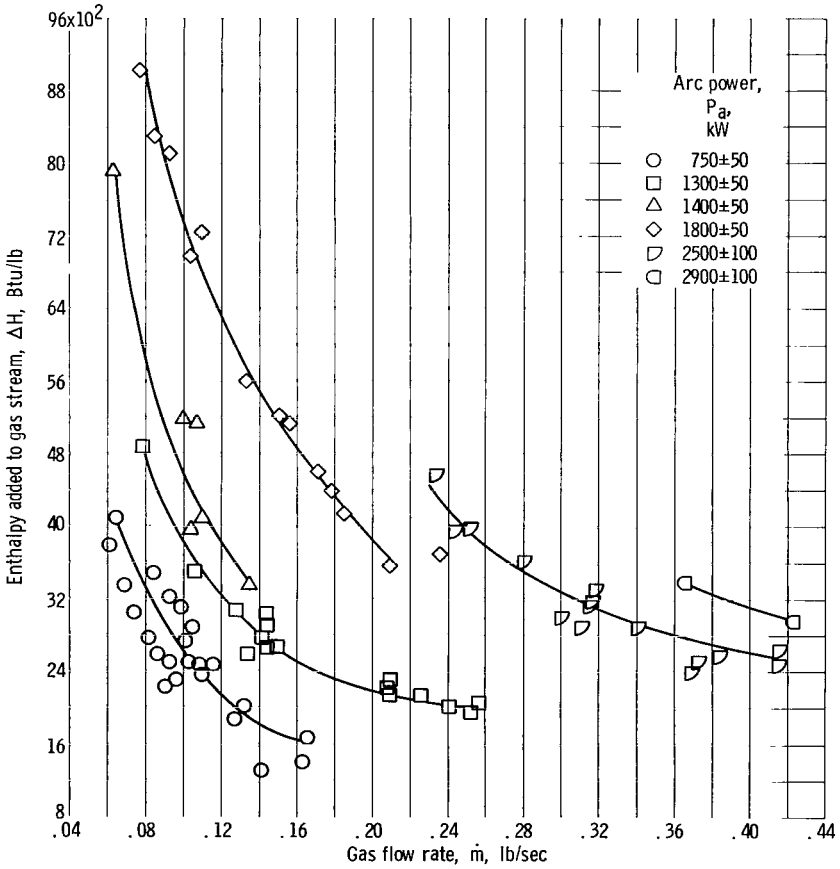

Figure 25. - Enthalpy as function of gas flow at constant arc power for ring cylinder.

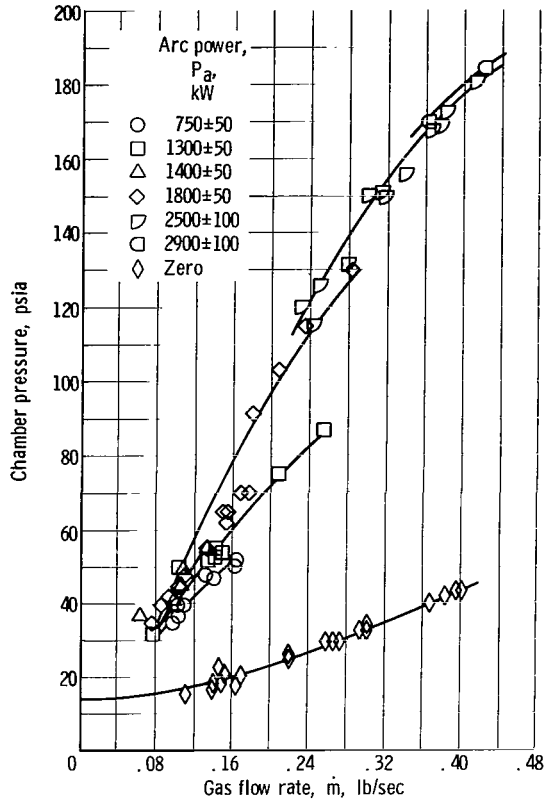

Figure 26. - Chamber pressure as function of flow rate at constant power.

gas flow during these tests was 0.42 pound per second. This maximum gas flow, with an arc power of 2.95 megawatts resulted in blow out of the arc and is presumed to be the gas flow limit for this power and arc length (1 in.).

Arc chamber pressures for the range of flows and arc powers investigated are shown in figure 26. The cold flow pressures for the same range of gas flows are also shown.

Observations

The ring-cylinder electrode configuration with the inner 4-inch ring fabricated from commercial copper pipe and a 6-inch inside-diameter anode as the cylinder electrode gave a 1-inch arc gap which permitted higher powers than the split-ring configuration. The ring-cylinder electrodes carried 7400 amperes without burnout and with these high currents did not blow out until flows of about 0.4 pound per second were reached. Maximum powers obtained were 3.0 megawatts in the arc and 1.2 megawatts in the gas.

Only one size of inner ring and hence only one arc length was investigated; however, it is expected that this gas flow limit could be increased with a larger ring and a smaller arc gap. With a selection of ring sizes it should be possible to cover quite a wide range of the desired gas power conditions.

COMPARISON OF ARC HEATERS

Each of the four types of heaters investigated failed to achieve the complete range of operation desired for the Lewis hypersonic arc tunnel; however, the evaluation indicated the feasibility of approaching the high enthalpy range (12 000 Btu/lb) with a combination of heaters incorporating the vortex-stabilized arc, and the low and intermediate enthalpy range (2000 to 8000 Btu/lb) with a ring-cylinder-type heater.

The capability of the arc heaters to simulate blunt-body stagnation point heat transfer can be estimated in terms of the mass flow rate and stagnation enthalpy for a given nozzle

configuration. Such an idealized comparison was made assuming the following:

(1) Nozzle area ratio, A/A*, of 256 with each heater

(2) Exhaust pressures sufficiently low to avoid nozzle flow separation

(3) Complete expansion (i.e., all of the thermal energy converted to kinetic energy at the nozzle exit)

(4) One-dimensional, steady, uniform flow

(5) Hemisphere-cylinder body shape

With these assumptions, stagnation point heat-transfer rates were computed from the following equations (refs. 11 and 12):

TABLE I. - COMPARISON OF ARC HEATERS FOR HYPERSONIC ARC TUNNEL

[Nozzle area ratio, A_e/A^*, 256.]

Arc heater	Throat diameter, d*, in.	Typical enthalpy investigated, Btu/lb	Correlated gas flow rate, lb/sec	Correlated arc chamber pressure, atm	Simulated heat-transfer rate, $Btu/(ft^2)(sec)$	Advantages	Disadvantages
Multiple chamber	0.75	6 000	0.06	2.0	$36.1/\sqrt{R}$	High power levels attainable from power-limited single heaters; good mixing in plenum	Geometrical complexity; cathode must operate in inert gas atmosphere; operation limited to relatively low chamber pressures ($p_0 < 3$ atm)
Vortex stabilized	1.0 .75	16 500 10 000	0.032 .035	1.0 1.5	$75.5/\sqrt{R}$ $54.6/\sqrt{R}$	High enthalpies at low pressure ($p_0 \simeq 1.0$ atm) and high arc current (I = 2000 to 3000 A); short gap permits spark starting	Cathode must operate in inert gas atmosphere
Split ring	0.75 .75	3 200 1 900	0.16 .40	5.0 10.0	$25.6/\sqrt{R}$ $20.5/\sqrt{R}$	Could heat air directly; high power levels; high pressure levels	Requires high cooling flows and pressures; must disassemble to insert starting wire
Ring cylinder	0.75 .75	7 200 2 900	0.10 .42	3.0 12.0	$59.5/\sqrt{R}$ $35.3/\sqrt{R}$	Could heat air directly; high power levels; high pressure levels	Requires high cooling flows and pressures; must disassemble to insert starting wire

$$q \simeq \frac{2.26\times10^{-2}}{\sqrt{R}} H_0^{1.075} \sqrt{p_{0,2}}$$

where

$$p_{0,2} = 3.29\times10^{-3}\left(\frac{\dot{m}}{A_e}\right)\sqrt{H_0}$$

and R is the hemispherical nose radius.

The computed stagnation-point heat-transfer rates and list of major advantages and disadvantages for each heater are presented in table I. The enthalpy, pressure, and flow rate corresponding to the computed heat-transfer rate are also listed. The vortex-stabilized and ring-cylinder heaters are found to produce nearly the same heat-transfer rate when each heater is operated with a 3/4-inch throat diameter nozzle. This result is because the lower enthalpy levels of the ring-cylinder heater are offset by much higher flow rates.

Table I also indicates the relatively high value of stagnation-point heat-transfer rate attainable with the vortex-stabilized arc heater operating with a 1.0-inch-diameter nozzle and atmospheric chamber pressure. Conversely, the high pressure performance of the split-ring and ring-cylinder heaters resulted in low values of stagnation enthalpy and, consequently, computed heat-transfer rates. These heater types appear to be more desirable where gas heating is necessary for simulation of aerodynamic, rather than heat-transfer phenomena.

CONCLUSIONS

The experimental evaluation of four arc heater design concepts has been conducted in order to determine the desirability of utilizing them for powering hypersonic arc tunnels. The evaluation indicated that the inherent performance limitations of the various heater designs may necessitate the use of more than one type of heater in order to cover a desired range of enthalpy and flow.

While only one basic geometry of each of the heater concepts was tested and all of the operating limits of the various arc parameters were not established, the results of this investigation indicate the following:

1. The performance of a multiple-chamber magnetically spun arc heater indicated the feasibility of clustering proven arc heater units onto a common plenum as a means of increasing gas power without an appreciable sacrifice in enthalpy levels. The magnetically spun arcs used in this investigation provided a nominal stagnation pressure and

enthalpy of 2 atmospheres and 5500 Btu per pound, respectively, with a 3/4-inch-diameter throat. Flow rates ranged from about 0.035 to 0.056 pound per second.

2. The vortex-stabilized arc provided a means of attaining a high gas enthalpy at a modest pressure level and low gas flow rate (16 500 Btu/lb at a pressure of 1 atm and a flow rate of 0.032 lb/sec). The upper level of pressure in this investigation was limited to about 5 atmospheres because of the power supply voltage limitation.

3. The split-ring and ring-cylinder electrode configurations investigated were capable of operating at gas flows of about 0.4 pound per second and pressures of about 10 atmospheres with gas enthalpies in the neighborhood of 3000 Btu per pound. These particular configurations offer considerable flexibility from the standpoint of ease in changing the arc gap to be compatible with gas power and gas flow requirements. Another attractive feature of ring electrodes is their ability to operate at high current levels.

Lewis Research Center,
National Aeronautics and Space Administration,
Cleveland, Ohio, January 13, 1966.

APPENDIX A

VOLTAGE CORRELATION FOR VORTEX-STABILIZED ARC

A voltage correlation can be obtained for the vortex-stabilized arc by modifying the dimensional correlation presented in reference 4 to include the influence of stagnation pressure. In order to apply the correlation the following basic assumptions are made:

1. The arc length is constant over the entire range of operating conditions. This is a reasonable assumption since the expansion section at the downstream end of the anode generally confined the length of the arc to approximately 7 inches.

2. The arc voltage for a given configuration is a function only of the current, mass flow rate, arc length, and electrical conductivity and specific enthalpy of the gas.

3. For a given stagnation pressure, the electrical conductivity and specific enthalpy of the gas do not influence the other parameters; that is, the temperature of the arc column changes only by a negligible amount.

In reference 4, an equation of the following form was generated:

$$I^a \dot{m}^b x^c \sigma^d H^e = C$$

which, upon substituting appropriate dimensions, becomes

$$(T^{-1}Q)^a (MT^{-1})^b L^c (M^{-1}L^{-3}TQ^2)^d (L^2T^{-2})^e = C$$

Reduction of this equation yields the nondimensional parameter

$$\varphi = \frac{I^2}{\dot{m}x\sigma H}$$

Similarly, replacing H by V requires the following expression to be dimensionless:

$$V^{a'} I^{b'} \dot{m}^{c'} x^{d'} \sigma^{e'} = C_1$$

When dimensions are substituted, the equation becomes

$$(ML^2T^{-2}Q^{-1})^{a'} (T^{-1}Q)^{b'} (MT^{-1})^{c'} L^{d'} (M^{-1}L^{-3}TQ^2)^{e'} = C_1$$

Reduction yields another nondimensional parameter:

$$\varphi_1 = VI^{-1}x\sigma$$

Hence,

$$f(\varphi, \varphi_1) = K$$

or

$$\frac{I^2}{\dot{m}x\sigma H} = f\left(\frac{Vx\sigma}{I}\right) \tag{A1}$$

Incorporation of assumption 3 as in reference 4 produces from (A1) a dimensional equation of the following form:

$$\frac{I^2}{\dot{m}x} = f_1\left(\frac{Vx}{I}\right) \tag{A2}$$

Since equation (A-2) is derived for constant pressure, it might be expected that a modification of the equation to include a pressure term would be feasible provided sufficient data are available to empirically prescribe the nature of the pressure variation. Constant pressure data were selected in the range of 0.8 to 3.0 atmospheres and plotted in figure 7 (p. 13) from which the following equation was derived:

$$\frac{I^2}{\dot{m}x} = 3.56\times10^7\left(\frac{Vx}{I}\right)^{-2.61} p_0^{0.338} \tag{A3}$$

APPENDIX B

SPLIT-RING FIELD CALCULATIONS

The self-induced magnetic field of the split-ring configuration may be estimated for any point along the arc element by considering the electrodes as filimentary conductors and applying the Biot-Savart relation

$$dB = \frac{I \sin \alpha \, ds}{10^3 r^2} \qquad \text{(B1)}$$

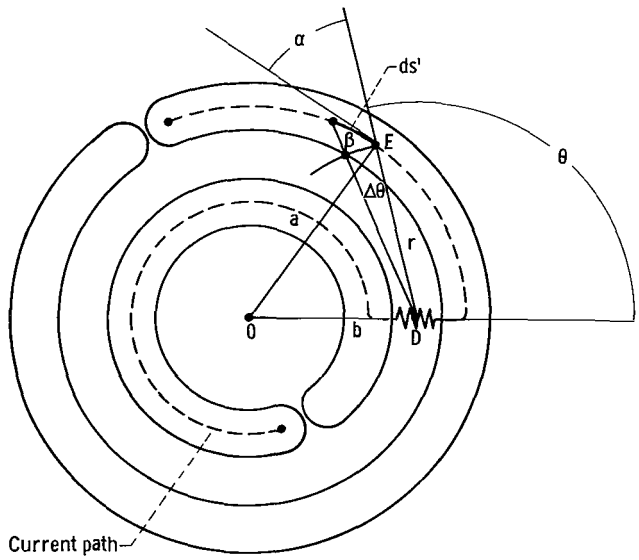

Figure 27. - Magnetic field at any point D inside a partial loop current.

(in the sense of fig. 27) for all current elements in the electrodes. The current in the stems was not considered, as the fields from the two stems would not effect the driving force on an arc in the plane of the rings.

Consider first the contribution of the partial loop current in the outer ring to the magnetic field at any point D inside a partial loop in the plane of the outer electrode as indicated in figure 27 (see also fig. 11, p. 16). From the geometry of figure 27,

$$ds \sin \alpha = ds \cos B \simeq r \, d\theta$$

so that equation (B1) becomes

$$dB = \frac{I \, d\theta}{10^3 r}$$

Therefore, magnetic field at point D is

$$B = \frac{I}{10^3} \int_0^{\theta} \frac{d\theta}{r}$$

Consider the triangle ODE:

$$a^2 = b^2 + r^2 - 2br \cos(180^\circ - \theta)$$

$$= b^2 + r^2 + 2br \cos \theta$$

$$r = \frac{-2b \cos\theta \pm \sqrt{4b^2 \cos^2\theta - 4(b^2 - a^2)}}{2}$$

$$= -b \cos\theta + a^2 - b^2 \sin^2\theta$$

Since r must be positive, therefore

$$B = \frac{I}{10^3} \int_0^{\theta} \frac{d\theta}{\sqrt{a^2 - b^2 \sin^2\theta} - b \cos\theta}$$

$$= \frac{I}{10^3} \int_0^{\theta} \frac{\left(\sqrt{a^2 - b^2 \sin^2\theta} + b \cos\theta\right) d\theta}{a^2 - b^2 \sin^2\theta - b^2 \cos^2\theta}$$

$$= \frac{I}{(a^2 - b^2)10^3} \int_0^{\theta} \left(\sqrt{a^2 - b^2 \sin^2\theta} + b \cos\theta\right) d\theta$$

Let $k = \frac{b}{a}$:

$$B = \frac{I}{(a^2 - b^2)10^3} \int_0^{\theta} \left(\sqrt{a^2 - a^2k^2 \sin^2\theta} + b \cos\theta\right) d\theta$$

$$= \frac{Ia10^{-3}}{a^2 - b^2} \int_0^{\theta} \sqrt{1 - k^2 \sin^2\theta}\, d\theta + \frac{Ib10^{-3}}{a^2 - b^2} \int_0^{\theta} \cos\theta\, d\theta$$

$$= \frac{Ia10^{-3}}{a^2 - b^2} E(k, \theta) + \frac{Ib10^{-3}}{a^2 - b^2} \sin\theta$$

where $E(k, \theta)$ is the elliptic integral of the second kind.

This expression was evaluated for the midpoint of the arc in the 0.54-inch-pipe electrode configuration for values of θ from 0^o to 360^o at 15^o increments and plotted against the appropriate value of arc position angle on the perimeter in figure 11 (p. 16).

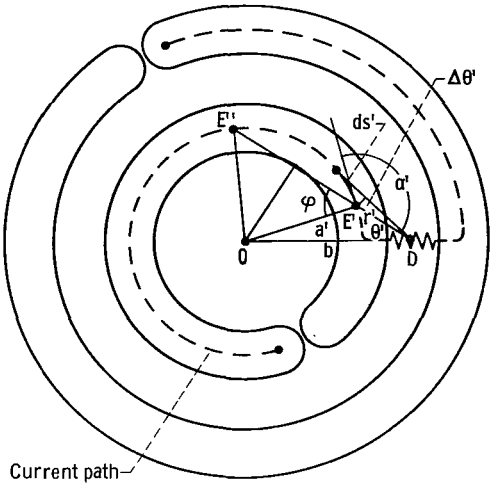

Figure 28. - Magnetic field at any point D outside a partial loop current.

In the same manner, the contribution to the field from the current in the inner ring was found (see fig. 28). From the geometry of figure 28,

$$ds' \sin \alpha' \cong ds' \cos(\alpha' - 90^{o}) \cong r' \, d\theta$$

so that equation (B1) becomes

$$dB' = \frac{I \, d\theta'}{10^3 r'}$$

Therefore,

$$B = \frac{I}{10^3} \int_0^{\theta'} \frac{d\theta'}{r'}$$

Let $b \sin \theta' = a' \sin \varphi$:

$$b \cos \theta' \, d\theta' = a' \cos \varphi \, d\varphi$$

Therefore,

$$\frac{d\theta'}{r'} = \frac{a' \cos \varphi \, d\varphi}{r' b \cos \theta'}$$

Consider the triangle ODE':

$$a'^2 = b^2 + r'^2 - 2r'b \cos \theta'$$

$$r' = b \cos \theta' - a' \cos \varphi$$

Therefore,

$$b^2 - a'^2 = 2r'b \cos \theta' - r' \cdot r'$$

$$= 2r'b \cos \theta' - r'b \cos \theta' + r'a' \cos \varphi$$

$$= r'b \cos \theta' + r'a' \cos \varphi$$

$$\frac{d\theta'}{r'} = \left(\frac{r'b \cos \theta' + r'a' \cos \varphi}{b^2 - a^2} \right) \frac{a' \cos \varphi \, d\varphi}{r'b \cos \theta'}$$

$$= \frac{1}{b^2 - a^2} \left(a' \cos \varphi \, d\varphi + \frac{a' \cos \varphi a' \cos \varphi \, d\varphi}{b \cos \theta'} \right)$$

$$B = \frac{I 10^{-3}}{b^2 - a^2} \left(\int_0^{\varphi} a' \cos \varphi \, d\varphi + \int_0^{\varphi} \frac{a' \cos \varphi a' \cos \varphi \, d\varphi}{b \cos \theta'} \right)$$

$$= \frac{I 10^{-3}}{b^2 - a^2} \int_0^{\varphi} \left(a' \cos \varphi + \frac{a'^2 - a'^2 \sin^2 \varphi}{b \sqrt{1 - \frac{a'^2}{b^2} \sin^2 \varphi}} \right) d\varphi$$

Let $k' = a'/b$:

$$B = \frac{Ib \, 10^{-7}}{b^2 - a^2} \int_0^{\varphi} \left(k' \cos \varphi + \frac{k'^2 - k'^2 \sin^2 \varphi}{\sqrt{1 - k'^2 \sin^2 \varphi}} \right) d\varphi$$

$$= \frac{I 10^{-3}}{b(1 - k'^2)} \left(\int_0^{\varphi} k' \cos \varphi \, d\varphi + \int_0^{\varphi} \frac{k'^2 - 1 + 1 - k^2 \sin^2 \varphi}{\sqrt{1 - k'^2 \sin^2 \varphi}} \, d\varphi \right)$$

$$= \frac{I}{b \, 10^3} \left[\frac{1}{1 - k'^2} \left(\int_0^{\varphi} k' \cos \varphi \, d\varphi + \int_0^{\varphi} \sqrt{1 - k'^2 \sin^2 \varphi} \, d\varphi \right) - \int_0^{\varphi} \frac{d\varphi}{\sqrt{1 - k'^2 \sin^2 \varphi}} \right]$$

$$= \frac{I}{b \, 10^3} \left\{ \frac{1}{1 - k'^2} \left[k' \sin \varphi + E(k', \varphi) \right] - F(k', \varphi) \right\}$$

where $E(k', \varphi)$ is the elliptic integral of the second kind and $F(k', \varphi)$ is the elliptic integral of the first kind.

This expression was also evaluated at the arc midpoint for the full cycle of values of φ, adjusted for arc position on the rings, and plotted in figure 11 (p. 16).

REFERENCES

1. Tillian, D.J.: Plasma Arc Facilities in the United States. Report No. 0-71000/3R-22. Ling-Temco-Vaught, Inc., Nov. 1963.

2. Boldman, Donald R.; Campbell, James P.; and Simon, Paul C.: Performance of Multiple-Chamber Arc Heater With Four Magnetically Spun Direct-Current Arcs. NASA TN D-2891, 1965.

3. Boldman, Donald R.; Shepard, Charles E.; and Fakan, John C.: Electrode Configurations for a Wind-Tunnel Heater Incorporating the Magnetically Spun Electric Arc. NASA TN D-1222, 1962.

4. Winovich, Warren: On the Equilibrium Sonic-Flow Method for Evaluating Electric-Arc Air-Heater Performance. NASA TN D-2132, 1964.

5. Kutateladze, S.S.; and Yasko, O.I.: Generalization of the Characteristics of Electric Arc Heaters. Inzhenerno-Fizicheskii Zhurnal, vol. VII, no. 4, 1964, pp. 25-27.

6. Shepard, Charles E.; Watson, Velvin R.; and Stine, Howard A.: Evaluation of a Constricted-Arc Supersonic Jet. NASA TN D-2066, 1964.

7. Ducati, Adriano C.; Giannini, Gabriel M.; and Muehlberger, Erich: Recent Progress in High Specific Impulse Thermo-Ionic Acceleration. Paper no. 65-27, AIAA, Jan. 1965.

8. Stine, Howard A.; and Watson, Velvin R.: The Theoretical Enthalpy Distribution of Air in Steady Flow Along the Axis of a Direct-Current Electric Arc. NASA TN D-1331, 1962.

9. Raezer, S.D.; Bunt, E.A.; and Olsen H.L.: Application of d.c. Plasma Arc Heating to Hypersonic Propulsion Testing. J. Spacecraft and Rockets, vol. 1, no. 2, Mar.-Apr. 1964, pp. 155-160.

10. Boldman, D.R.: Performance Evaluation of a Magnetically Spun D.C. Arc Operating in Nitrogen. AIAA J., vol. 1, no. 4, Apr. 1963, pp. 802-805.

11. Detra, R.W.; Kemp, N.H.; and Riddell, F.R.: Addendum to Heat Transfer to Satellite Vehicles Reentering the Atmosphere. Jet Propulsion, vol. 27, no. 12, Dec. 1957, pp. 1256-1257.

12. Shepard, C.E.; and Winovich, Warren: Electric-Arc Jets for Producing Gas Streams with Negligible Contamination. Paper No. 61-WA-247, ASME, Nov-Dec., 1961.

"The aeronautical and space activities of the United States shall be conducted so as to contribute . . . to the expansion of human knowledge of phenomena in the atmosphere and space. The Administration shall provide for the widest practicable and appropriate dissemination of information concerning its activities and the results thereof."

—NATIONAL AERONAUTICS AND SPACE ACT OF 1958

NASA SCIENTIFIC AND TECHNICAL PUBLICATIONS

TECHNICAL REPORTS: Scientific and technical information considered important, complete, and a lasting contribution to existing knowledge.

TECHNICAL NOTES: Information less broad in scope but nevertheless of importance as a contribution to existing knowledge.

TECHNICAL MEMORANDUMS: Information receiving limited distribution because of preliminary data, security classification, or other reasons.

CONTRACTOR REPORTS: Technical information generated in connection with a NASA contract or grant and released under NASA auspices.

TECHNICAL TRANSLATIONS: Information published in a foreign language considered to merit NASA distribution in English.

TECHNICAL REPRINTS: Information derived from NASA activities and initially published in the form of journal articles.

SPECIAL PUBLICATIONS: Information derived from or of value to NASA activities but not necessarily reporting the results of individual NASA-programmed scientific efforts. Publications include conference proceedings, monographs, data compilations, handbooks, sourcebooks, and special bibliographies.

Details on the availability of these publications may be obtained from:

SCIENTIFIC AND TECHNICAL INFORMATION DIVISION

NATIONAL AERONAUTICS AND SPACE ADMINISTRATION

Washington, D.C. 20546